Flow Characterizations and Drag Reduction on the Hydrophobic Surface with a Full Covering Gas Film

P. Du[1,2], D. Song[1], F. Ren[1], Q. Xue[3] and H. Hu[1,4†]

[1] *School of Marine Science and Technology, Northwestern Polytechnical University, Xi'an, Shaanxi, 710072, People's Republic of China*
[2] *Sorbonne Universities, University of Technology of Compiegne, Lab. Roberval, UMR 7337 CNRS Centre de recherches Royallieu BP 20529, 60206 Compiegne Cedex, France*
[3] *Ningbo Institute of Materials Technology & Engineering, Chinese Academy of Sciences, Ningbo, Zhejiang, 315201, People's Republic of China*
[4] *The Institute of NPU in Shenzhen, Northwestern Polytechnical University, Shenzhen 518057, Peoples Republic of China*

†*Corresponding Author Email: huhaibao@nwpu.edu.cn*

ABSTRACT

Characteristics of the flow on hydrophobic surfaces with a full covering gas film are investigated using the single-component multi-phase (SCMP) Lattice Boltzmann (LB) simulation. By adopting the Shan-Doolen force model and incorporating equations of state (EOS) of real fluids, large density ratios are achieved. The height of the air film maintained is observed to increase with the improvement of the surface hydrophobicity. In the laminar flow, the state of the gas-liquid interface is not influenced by the Reynolds number (Re). On the gas layer, the slip effect and wall shear stress reduction are sustained continuously regardless of their positions (on the space or on the micro-structure). Even so, decreasing the solid area fraction is also significant to enhance the slip effect and decrease the wall shear stress on hydrophobic surfaces.

Keywords: Hydrophobic surface; Lattice Boltzmann method; Gas film; Slip; Drag reduction.

NOMENCLATURE

$\mathbf{a}$	acceleration	$\mathbf{u}$	velocity
CA	contact angle	u_s	slip velocity
c_s	lattice sound speed	w	width of micro-structure
c	lattice speed		
$\mathbf{e}_\alpha$	discrete velocity	f	velocity distribution function
G_s	fluid-solid interaction strength	δ_t	time step
G	interparticle strength	τ	single relaxation time
h	height of micro-structure	ω_α	weighting factor
H	height of gas-liquid interface	δ_x	spatial step
L_s	slip length	ρ	density
p	pressure	v	kinetic viscosity
Re	Reynolds number	f_x	driving force
s	width of space between micro-structures	τ_ω	wall shear stress
swi	switch function	f_s	space ratio
T	temperature		

1. INTRODUCTION

Hydrophobic surface is a new technique to reduce the frictional drag, whose effect has been proved in many studies (Haibao, Peng, Feng, Dong, and Yang 2015; Martell, Perot, and Rothstein 2009; Min and Kim 2004; Ou and Rothstein 2005; Tretheway and Meinhart 2002). As for the mechanism, most researchers consider an air-water interface existing between micro-structures, on which the shear is

sharply decreased and the slip is formed (Choi, Ulmanella, Kim, Ho, and Kim 2006; Martell, Perot, and Rothstein 2009; Ou and Rothstein 2005; Park, Park, and Kim 2013; Samaha, Tafreshi, and Gad-el Hak 2011; Tretheway and Meinhart 2002). Ou *et al.* (2005) conducted direct velocity measurements of the flow on hydrophobic surfaces using $\mu - PIV$ and discovered that an air-water interface was sup-ported between ridges; the slip velocity at the center of the interface reached 60% of the average velocity in the microchannel. Martell *et al.* (2009) established a model of hydrophobic surfaces using Direct Numerical Simulations (DNS), with a free surface interface between micro-ridges and posts. The wall shear stress reduction was found to be nearly 40%. Song *et al.* (Song, Daniello, and Rothstein 2014) conducted experiments for the laminar flow of water through microchannels using hydrophobic surfaces. A maximum slip length of 20 μm was obtained and a correlation between the slip length and the contact angle hysteresis was found. Choi *et al.* (Choi, Ulmanella, Kim, Ho, and Kim 2006) reported the effective slip and drag reduction in hydrophobic microchannels. A noticeable slip of 100-200 nm generated by the nanostrips of air was observed. This surface would not only reduce friction in liquid flows but also enable directional control of the slip.

However, inconsistent with former studies, gas was found to not only exist between micro-structures, but formed a film and covered the whole surface (Fig. 1). Sheng *et al.* (2011) observed this phenomenon on a lotus leaf placed underwater. The gas layer was found to become unstable and even disappeared when the hydraulic pressure was in-creased. Yu *et al.* (Yong-Sheng and Qing-Ding 2006) also observed air layers in macroscopic size on hydrophobic surfaces, which can cause apparent velocity slip for the drag reduction. Gao *et al.* (2009) performed numerical simulations of the shear flow over periodically patterned substrates. A continuous gas film was formed when the shear rate was larger than a critical value, resulting in an enhanced slip length proportional to the liquid-gas viscosity ratio. Fukuda *et al.* (Fukuda, Tokunaga, Nobunaga, Nakatani, Iwasaki, and Kunitake 2000) tested the effect of hydrophobic surfaces with an air film using ship models. A drag reduction up to 80%was obtained. After all, relative studies are still in-sufficient and the effect of this air film needs further investigations.

As a new simulation technique, especially in the hydrophobic field, Lattice Boltzmann (LB) method showed great applicability (Hao and Cheng 2009; Harting, Kunert, and Hyväluoma 2010; Moradi, Varnik, and Steinbach 2010; Zhu, Tretheway, Petzold, and Meinhart 2005; Aidun and Clausen 2010). The pseudo-potential model proposed by Shan and Chen (1993) can be used to simulate the single-component multi-phase (SCMP) problem; thus the fluid-fluid interaction and fluid-solid interaction can be adjusted, which are in accordance with the properties of the fluid and solid wall in the practical situation. Based on this model, Cui *et al.* (2011) investigated the fluid flows through channels with different wettability conditions and topographical surfaces. They found that the rough

ness has a positive effect for reducing the pressure drop on hydrophobic surfaces. Harting *et al.* (2006) simulated the flow in hydrophobic rough microchannels and discovered that the roughness created a non-linear effect for the slip length.
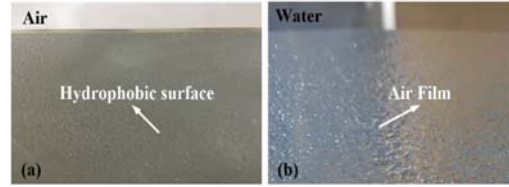
Fig. 1. Comparison of hydrophobic surfaces (a) in the air and (b) under water. There exists an air film in (b) covering the whole surface.

In this paper, multi-phase flows with a gas film on hydrophobic surfaces were simulated using LB method. An equation of state (EOS) was incorporated to improve the density ratio and decrease spurious currents. The state of the gas film, the slip effect and the shear stress changing with the solid-liquid interaction, the flow speed and micro-structures were analyzed to characterize the proper-ties of this flow.

2. METHODOLOGY

2.1 SCMP Lattice Boltzmann Model

The concept of the LB method is to calculate the probability at a certain state of each particle, and then get the macroscopic parameters statistically. The basic equation of the LB method (He and Luo 1997a; He and Luo 1997b; Chen and Doolen 1998; Succi 2001; Swift, Osborn, and Yeomans 1995; He, Chen, and Zhang 1999) is

$$f_\alpha(\mathbf{x} + \mathbf{e}_\alpha \delta_t, t + \delta_t) - f_\alpha(\mathbf{x}, t) = -\frac{1}{\tau}[f_\alpha(\mathbf{x},t) - f_\alpha^{eq}(\mathbf{x},t)] \tag{1}$$

where fαeq is the local equilibrium velocity dis-tribution function. The macroscopic state is the collective behavior of particles' velocity distribution functions. In this study, the D2Q9 model is applied (Qian, d'Humi`eres, and Lallemand 1992). The equilibrium velocity distribution of the D2Q9 model can be expressed as

$$f_\alpha^{eq} = \rho \omega_\alpha [1 + \frac{\mathbf{e}_\alpha \mathbf{u}}{c_s^2} + \frac{(\mathbf{e}_\alpha \mathbf{u})^2}{2c_s^4} + \frac{u^2}{2c_s^2}] \tag{2}$$

where the weighting factor ωα, the discrete velocity eα and the lattice sound speed cs are defined as

$$\omega_\alpha = \begin{cases} 4/9 & \alpha = 0 \\ 1/9 & \alpha = 1,2,3,4 \\ 1/36 & \alpha = 5,6,7,8 \end{cases} \tag{3}$$

$$[\mathbf{e}_0, \mathbf{e}_1, \mathbf{e}_2, \mathbf{e}_3, \mathbf{e}_4, \mathbf{e}_5, \mathbf{e}_6, \mathbf{e}_7, \mathbf{e}_8] = \begin{bmatrix} 0 & 1 & 0 & -1 & 0 & 1 & -1 & -1 & 1 \\ 0 & 0 & 1 & 0 & -1 & 1 & 1 & -1 & -1 \end{bmatrix} \tag{4}$$

$$c_s = \frac{c}{\sqrt{3}} \qquad (5)$$

where the lattice speed $c = \delta_x / \delta_t$. The macroscopic variables are defined as

$$(6) \quad \rho = \sum_\alpha f_\alpha$$

$$\mathbf{u} = \frac{1}{\rho} \sum_\alpha \mathbf{e}_\alpha f_\alpha \qquad (7)$$

$$p = \rho c_s^2 \qquad (8)$$

$$v = c_s^2 (\tau - \frac{1}{2}) \delta_t \qquad (9)$$

The pseudo-potential model is applied simulating the SCMP flow in this study. For the D2Q9 model, the interaction force between the particle at the site x and the particles around is expressed as

$$\mathbf{F}_{int}(\mathbf{x},t) = -G\Psi(\mathbf{x},t) \sum_{\alpha=1}^{8} \omega_\alpha \Psi(\mathbf{x} + \mathbf{e}_\alpha \delta_t, t) \mathbf{e}_\alpha \qquad (10)$$

where $\Psi(\mathbf{x},t)$ is the effective mass, which is a function of the density. According to this equation, $\mathbf{F}_{int}$ is generated by the difference of $\Psi(\mathbf{x},t)$, i.e. the density ρ. When the density of the neighboring par-ticles are the same, $\mathbf{F}_{int}$ will be 0.

The interaction force between fluid particles and the solid surface is expressed as (Martys and Chen 1996)

$$\mathbf{F}_{ads}(\mathbf{x},t) = -G_s \rho(\mathbf{x},t) \sum_{\alpha=1}^{8} \omega_\alpha swi(\mathbf{x} + \mathbf{e}_\alpha \delta_t, t) \mathbf{e}_\alpha \qquad (11)$$

The wettability of solid surfaces can be controlled by changing the fluid-solid interaction strength G_s. The switch function *swi* will be 1 or 0 when the site $(\mathbf{x} + \mathbf{e}_\alpha \delta_t)$ is solid or fluid.

2.2 Force Model and Boundary Conditions

The equations of the interaction force have been shown in Section 2.1. However, they should be further incorporated into the evolution of the LB equation. During the simulation, the interaction forces of (10) and (11) are incorporated by replacing the velocity $\mathbf{u}$ with the equilibrium velocity $\mathbf{u}_{eq}$ in the equilibrium distribution function (2)

$$\mathbf{u}_{eq} = \mathbf{u} + \mathbf{a}\tau\delta_t \qquad (12)$$

where the acceleration a can be calculated as $\mathbf{a} = \mathbf{F} / \rho$. External forces can also be incorporated through the same process.

The macroscopic velocity in Eq. (7) is corrected using the average velocity before and after a collision step uave according to the Shan-Doolen model (Shan and Doolen 1995),

$$\mathbf{u}_{ave} = \frac{1}{2}(\mathbf{u} + \mathbf{u}') = \frac{1}{\rho}\left(\sum_i \mathbf{e}_\alpha f_i + \frac{\delta_t}{2}\mathbf{F} \right) \qquad (13)$$

For the fluid area, the periodic boundary is adopted during the simulation. For the solid wall, the halfway bounce-back boundary is adopted, which has been proved to have second-order accuracy (He, Zou, Luo, and Dembo 1997).

2.3 Incorporating Equations of State

By correlating Eq. (1) with Navier-Stokes equations through the Chapman-Enskog expansion (Shan and Chen 1993), the EOS for the pseudo-potential model can be obtained.

$$p = \rho c_s^2 + \frac{G}{6}\Psi^2(\rho) \qquad (14)$$

which is a non-ideal gas EOS. cs is the lattice sound speed. The EOS (Yuan and Schaefer 2006) describes the relation of pressure, temperature and density. By substituting various EOSs of real fluids into this equation, different EOSs for the LB method can be obtained. The modified Kaplun Meshalkin (mKM) EOS (Kupershtokh, Medvedev, and Karpov 2009) is applied in this study.

$$\tilde{p} = \tilde{c}\tilde{\rho}\tilde{T}(1 + \frac{\tilde{d}}{1/\tilde{\rho}} - \tilde{b}) - \tilde{a}\tilde{\rho}^2 \mathbf{g} \qquad (15)$$

To satisfy the critical point conditions (Chen, Zhong, and Yuan 2011),

$$\tilde{\rho} = 1 \quad \tilde{T} = 1 \quad \tilde{p} = 1$$
$$(\frac{\partial \tilde{p}}{\partial \tilde{\rho}})_{\tilde{T}} = 0 \quad (\frac{\partial^2 \tilde{p}}{\partial \tilde{\rho}^2})_{\tilde{T}} = 0 \qquad (16)$$

the parameters are calculated as

$$\tilde{a} = \frac{1}{3 - \tilde{c}} \quad \tilde{b} = 3 - \tilde{c} \quad \tilde{d} = \frac{12\tilde{c} - 6\tilde{c}^2 + \tilde{c}^3 - 8}{\tilde{c}(3 - \tilde{c})} \qquad (17)$$

According to the work of Kupershtokh (Kupershtokh, Medvedev, and Karpov 2009), the value $\tilde{c} = 2.78$ should be chosen to best agree with the experimental data. So the values of the variables are

$$\tilde{a} = 4.5455 \quad \tilde{b} = 0.22 \quad \tilde{c} = 2.78 \quad \tilde{d} = 0.7759$$

When $\tilde{T} < 1$, two phases can coexist. To incorporate the mKM EOS, Eq. (14) should be changed to

$$\Psi(\rho) = \sqrt{\frac{6(p - \rho/3)}{G}} \qquad (18)$$

It can be seen that the incorporated EOS functions indirectly through the effective mass ψ. During the evolution, the fluid-fluid interaction G will be crossed out; instead, the temperature T will function and affect the interaction between fluid particles, which is in accordance with the practical situation. By incorporating the mKM EOS, large density ratios are obtained. In this paper, the temperature $\tilde{T} = 0.63$ is adopted and the corresponding density ratio is about 1500.

3. PREPARATION OF SIMULATION

3.1 Characterization of Wettability

The wettability of the solid surface is always evaluated using the intrinsic contact angle (*CA*) (Song, Daniello, and Rothstein 2014; Song, Song, Hu, Du, and Ma 2015). In the LB simulation, there are three factors affecting the *CA*, i.e. the temperature, the solid-liquid interaction and surface structures. The temperature influences the surface tension, in this study, the surface tension is already known (about 0.187) because the temperature has been fixed as in Section 2.3. The solid-liquid interaction and surface structures correspond to the surface energy and the roughness of real solid surfaces (Yao, Hao, Zhang, and He 2012).

The effect of the solid-liquid interaction G_s can be obtained by simulating a liquid drop under different G_s on the smooth surface. As seen in Fig. 2, with de-creasing $|G_s|$, the interaction between the wall and the fluid drops, and so the *CA*s increase. On the smooth surface, the *CA* and the solid-liquid interaction show a linear relation ($y = 440.04 + 157.4x$). This phenomenon is consistent with former studies (Cui, Li, and Lam 2011). Here, when $||G_s| \leq 2.2$, $CA \leq 90°$, the surface is hydrophobic.

3.2 Computational Domain

As introduced in Section 1., instead of only existing between micro-structures, the air layer is also observed covering the entire hydrophobic surface, i.e. the solid wall contact indirectly with water. The effect of this air film needs to be characterized. According to this phenomenon, a LB model is established. Fig. 5 shows the initial state of the LB simulation. A gas layer covers the entire solid surface, including the top of micro-structures. The bottom wall is structured, while the top wall is smooth for comparison.
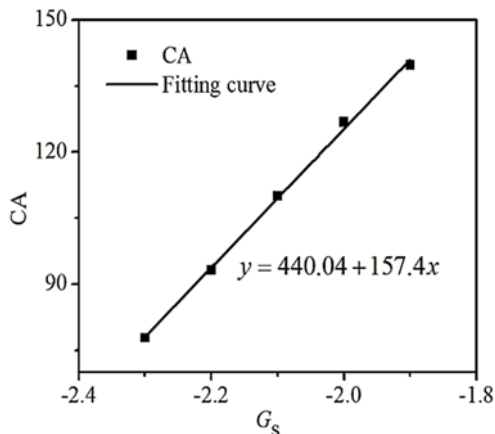

Fig. 2. Relation between the contact angle (*CA*) and the solid-liquid interaction (G_s).

4. RESULTS AND DISCUSSIONS

According to the initial model in Fig. 3, the sys-tem is controlled to evolve under different solid liquid interactions G_s statically (without outer interferences). When the system is balanced, the height of the gas-liquid interface H is extracted. As seen in Fig. 4, when the wall shows good hydrophobicity ($|G_s| < 2.2$), the gas-liquid interface can be sustained steadily. On both the spaces and the micro-structures, the height of the interface held increases with improving surface hydrophobicity. Because of the support of hydrophobic pillars, the height of the interface in the spaces is much thicker than that over the micro-structures. When the wall is hydrophilic ($|G_s| \geq 2.2$), the liquid will enter into the spaces.
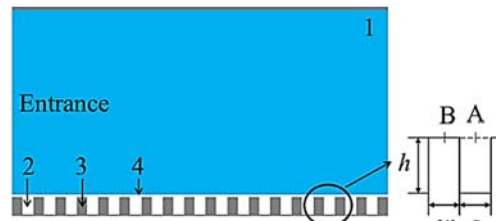

Fig. 3. Lattice Boltzmann model of hydrophobic surfaces with a gas film: (1) liquid; (2) gas; (3) solid; (4) gas-liquid interface. A is the midpoint of the space. B is the midpoint of the top of the micro-structure.
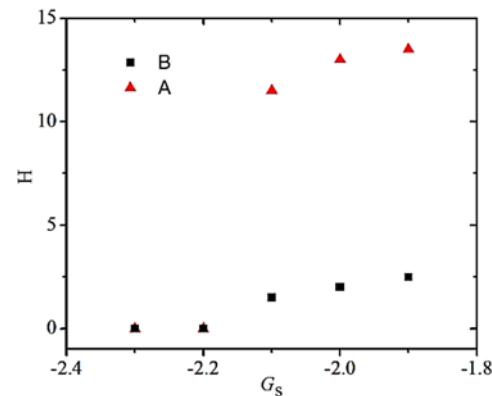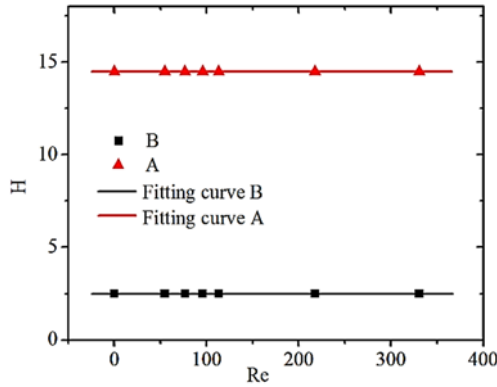

Fig. 4. Height of the gas-liquid interface (*H*) sustained at position A (midpoint of the space) and B (midpoint of the micro-structure) with different solid-liquid interactions (G_s).

Good hydrophobicity is seen to be crucial for the maintenance of the gas-liquid interface. High interface will weaken the restriction of the wall and accelerate the neighboring fluids, which will benefit the formation of the slip on hydrophobic surfaces.

To investigate the properties of the gas layer dynamically, the system is controlled to evolve as the static state at first. When the air layer becomes steady, different forces f_x are added at the entrance of the channel (see Fig. 3) to drive the flow. The

corresponding Reynolds numbers *Re* are 54.81, 76.56, 95.7, 113.1, 217.5 and 330.6 when the system is balanced. Continuing increasing Re will cause the computational divergence, so the flows in this paper are in the laminar state. The height of the gas layer *H* is also extracted. Fig. 5 shows that *H* at different *Re* are completely the same, regardless of the positions on the spaces or over the micro-structures.

Fig. 5. Height of the gas-liquid interface (*H*) sustained at position A (midpoint of the space) and B (midpoint of the micro-structure) with different Reynolds numbers (*Re*).

This phenomenon demonstrates that, in the laminar state, the flow speed will not influence the state of the gas liquid interface.

The velocity profiles at the middle of the space and the micro-structure, i.e. position A and B in Fig. 3, are extracted. In Fig. 6, a lifting-up phenomenon can be observed in the near-wall region (Zhang, Tian, Yao, Hao, and Jiang 2015; Tian, Zhang, Jiang, and Yao 2015). On the hydrophobic surface, the existence of the air film and the low surface energy weaken the wall's restriction to the fluids, so the fluids are accelerated compared with that on the smooth surface, which forms the slip on the gas liquid interface. This effect has been confirmed in both experimental and numerical studies previously (Choi, Ulmanella, Kim, Ho, and Kim 2006; Ou and Rothstein 2005; Park, Park, and Kim 2013; Samaha, Tafreshi, and Gadel Hak 2011). But un-like these works, because of the full covering of the gas layer in this study, the velocity profiles over the two positions are close, which demonstrates that a full gas layer can maintain the acceleration of fluid particles continuously. The continuous slip can then be formed along the gas-liquid interface, thus benefits the drag reduction on hydrophobic surfaces.

By fitting the velocity profile, slip parameters can be calculated. The definition of the slip is shown in Fig. 7, which is deduced from Navier's model (Rothstein 2010):

$$u_s = L_s \frac{du}{dy}\bigg|_{wall} \tag{19}$$

The slip velocity u_s and the slip length L_s are connected by the velocity gradient at the wall

$\frac{du}{dy}\bigg|_{wall}$. Table 1 shows that the slip exists on both the spaces and the micro-structures as pointed in Fig. 6. The slip velocity increases with increasing Reynolds number *Re*. Because the gas-liquid interface is closer to the top of the micro-structure, the inter-action between liquids and the wall is stronger. The nearby fluids will be more restrained, so the slip velocity over the micro-structure is lower than that over the space. The largest slip velocity over the micro-structure and the space reaches 7.92% and 5.65% of the central flow, respectively. The slip lengths of the two are nearly the same. This demonstrates that, with an air film, the slip will be maintained continuously on the gas-liquid interface, regardless of the position over the wall. According to Newton's law of viscosity, wall shear stresses on the smooth and hydrophobic surfaces can be calculated.

$$\tau_\omega = \mu \frac{du}{dy}\bigg|_{wall} \tag{20}$$
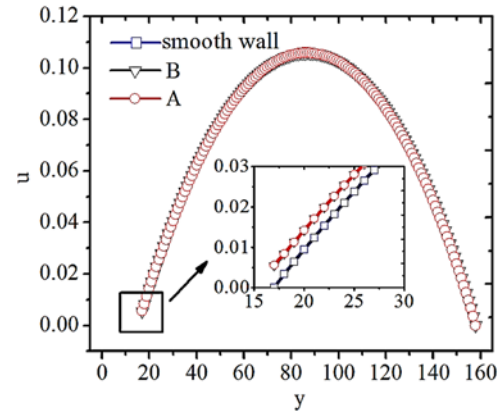
Fig. 6. Velocity profiles when *Re* = 95.7 on the smooth surface and position A (midpoint of the space) and B (midpoint of the micro-structure) of the hydrophobic surface.
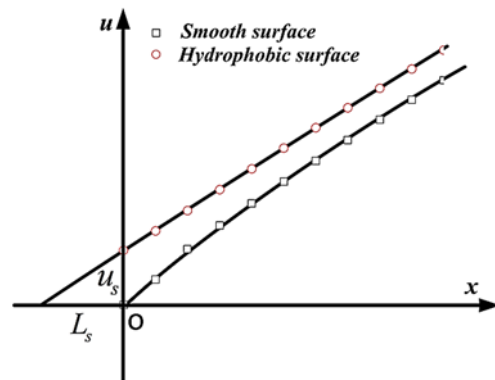
Fig. 7. Sketch of the slip on the hydrophobic surface.

The velocity gradient at the wall $\frac{du}{dy}\bigg|_{wall}$ can be obtained from the slip Eq. (19). The detailed

Table 1 Slip parameters and wall shear stresses on the smooth surface and position A (midpoint of the space) and B (midpoint of the micro-structure) of the hydrophobic surface

	smooth surface	A			B		
Re	$\tau_\omega \times 10^3$	$u_s \times 10^2$	L_s	$\tau_\omega \times 10^3$	$u_s \times 10^2$	L_s	$\tau_\omega \times 10^3$
54.81	0.699	0.499	2.804	0.599	0.356	2.689	0.381
75.56	0.883	0.634	2.840	0.703	0.469	2.756	0.489
95.7	1.084	0.769	2.649	0.915	0.581	2.746	0.609
113.1	1.170	0.837	2.799	0.942	0.637	2.769	0.662
217.5	1.974	1.509	2.739	1.743	1.199	2.724	1.264
330.6	2.936	2.171	2.710	2.549	1.760	2.719	1.856

calculation process can refer to (Haibao, Peng, Feng, Dong, and Yang 2015). Normally, the wall shear stress can be used to represent the frictional drag on the wall. In Table 1, the shear stresses on both positions of the hydrophobic surface are lower than that on the smooth surface, which proves that the gas film is able to reduce the frictional drag on the entire hydrophobic surface.

To further investigate the effect of micro-structures, three solid area fractions $f_s = \dfrac{w}{s+w}$ were designed, 66.67%, 50.00% and 33.33%, with the solid-liquid interaction G_s −1.9 and the Reynolds number Re 95.7. Table 2 indicates that, both the slip velocity and the slip length increase as the solid fraction de-clines, because the influence of the wall is further weakened, which results in stronger acceleration of near-wall fluids and higher up-lifting of the velocity profile. The wall shear stress also drops with decreasing solid area fraction. So, smaller solid area fraction benefits the slip and the drag reducing effect on the hydrophobic surface, even with a full-covering gas film.

Table 2 Slip parameters and wall shear stresses with different solid area fractions.

f_s	66.67%	50.00%	33.33%
$u_s \times 10^2$	0.693	0.769	1.532
L_s	1.985	2.649	5.352
$\tau_\omega \times 10^3$	1.136	0.915	0.711

5. CONCLUSION

Based on the recognition of a full covering air film on the hydrophobic surface, a new numerical model was established using LB method correspondingly. During the simulation, the SCMP LB method was adopted. By employing the Shan-Doolen force model and incorporating the mKM EOS, large density ratios were achieved in the study. The conclusions can be drawn as follows:

(1) Hydrophilic surfaces are not able to maintain the gas layer on the wall. The height of the gas film sustained increases with improving surface hydrophobicity. In the laminar flow, the state of the gas film is not influenced by the Reynolds number Re.

(2) The air film can reduce the difference of velocity

fields over the micro-structure and the space between micro-structures. The slip effect and the wall shear stress reduction are achieved continuously on the entire hydrophobic surface.

(3) Small solid area fraction is beneficial to increase the slip and decrease the wall shear stress. So even on the hydrophobic surface with a full covering air film, the optimization of micro-structures is also required to achieve good drag reducing effect.

REFERENCES

Aidun, C. K. and J. R. Clausen (2010). Lattice-Boltzmann method for complex flows. *Annual Review of Fluid Mechanics* 42, 439-472.

Chen, S. and G. D. Doolen (1998). Lattice Boltzmann method for fluid flows. *Annual Review of Fluid Mechanics* 30(1), 329-364.

Chen, X. P., C. W. Zhong and X. L. Yuan (2011). Lattice Boltzmann simulation of cavitating bubble growth with large density ratio. *Computers and Mathematics with Applications* 61(12), 3577-3584.

Choi, C. H., U. Ulmanella, J. Kim, C. M. Ho and C. J. Kim (2006). Effective slip and friction reduction in nanograted superhydrophobic microchannels. *Physics of Fluids* 18(8).

Cui, J., W. Li and W. H. Lam (2011). Numerical investigation on drag reduction with superhydrophobic surfaces by lattice-Boltzmann method. *Computers and Mathematics with Applications* 61(12), 3678-3689.

Fukuda, K., J. Tokunaga, T. Nobunaga, T. Nakatani, T. Iwasaki and Y. Kunitake (2000). Frictional drag reduction with air lubricant over a super-water-repellent surface. *Journal of Marine*

Science and Technology 5(3), 123-130.

Gao, P. and J. J. Feng (2009). Enhanced slip on a patterned substrate due to depinning of contact line. *Physics of Fluids* 21(10).

Haibao, H., D. Peng, Z. Feng, S. Dong and W. Yang (2015). Effect of hydrophobicity on turbulent boundary layer under water. *Experimental Thermal and Fluid Science* 60, 148-156.

Hao, L. and P. Cheng (2009). Lattice Boltzmann simulations of liquid droplet dynamic behavior on a hydrophobic surface of a gas flow channel. *Journal of Power Sources* 190(2), 435-446.

Harting, J., C. Kunert and H. J. Herrmann (2006). Lattice Boltzmann simulations of apparent slip in hydrophobic microchannels. *Europhysics Letters* 75(2), 328.

Harting, J., C. Kunert and J. Hyväluoma (2010). Lattice Boltzmann simulations in microfluidics: probing the no-slip boundary condition in hydrophobic, rough, and surface nanobubble laden microchannels. *Microfluidics and Nanofluidics* 8(1), 1-10.

He, X. and L. S. Luo (1997a). A priori derivation of the lattice Boltzmann equation. *Physical Review E* 55(6).

He, X. and L. S. Luo (1997b). Theory of the lattice Boltzmann method: From the Boltzmann equation to the lattice Boltzmann equation. *Physical Review E* 56(6).

He, X., Q. Zou, L. S. Luo and M. Dembo (1997). Analytic solutions of simple flows and analysis of nonslip boundary conditions for the lattice Boltzmann BGK model. *Journal of Statistical Physics* 87(1-2), 115-136.

He, X., S. Chen, and R. Zhang (1999). A lattice Boltzmann scheme for incompressible multiphase flow and its application in simulation of Rayleigh–Taylor instability. *Journal of Computational Physics* 152(2), 642-663.

Kupershtokh, A. L., D. A. Medvedev and D. I. Karpov (2009). On equations of state in a lattice Boltzmann method. *Computers and Mathematics with Applications* 58(5), 965-974.

Martell, M. B., J. B. Perot and J. P. Rothstein (2009). Direct numerical simulations of turbulent flows over superhydrophobic surfaces. *Journal of Fluid Mechanics* 620, 31–41.

Martys, N. S. and H. Chen (1996). Simulation of multicomponent fluids in complex three-dimensional geometries by the lattice Boltzmann method. *Physical Review E* 53(1).

Min, T. and J. Kim (2004). Effects of hydrophobic surface on skin-friction drag. *Physics of Fluids* 16(7), L55–L58.

Moradi, N., F. Varnik, and I. Steinbach (2010). Roughness-gradientinduced spontaneous motion of droplets on hydrophobic surfaces: A lattice Boltzmann study. *Europhysics Letters* 89(2).

Ou, J. and J. P. Rothstein (2005). Direct velocity measurements of the flow past drag-reducing ultrahydrophobic surfaces. *Physics of Fluids* 17(10).

Park, H., H. Park and J. Kim (2013). A numerical study of the effects of superhydrophobic surface on skin-friction drag in turbulent channel flow. *Physics of Fluids* 25(11).

Qian, Y. H., D. d'Humières and P. Lallemand (1992). Lattice bgk models for navier-stokes equation. *Europhysics Letters* 17(6).

Rothstein, J. P. (2010). Slip on superhydrophobic surfaces. *Annual Review of Fluid Mechanics* 42, 89-109.

Samaha, M. A., H. V. Tafreshi and M. Gad-el-Hak (2011). Modeling drag reduction and meniscus stability of superhydrophobic surfaces comprised of random roughness. *Annual Review of Fluid Mechanics* 23(1).

Shan, X. and G. Doolen (1995). Multicomponent lattice-Boltzmann model with interparticle interaction. *Journal of Statistical Physics* 81(1-2), 379-393.

Shan, X. and H. Chen (1993). Lattice Boltzmann model for simulating flows with multiple phases and components. *Physical Review E* 47(3).

Sheng, X. and J. Zhang (2011). Air layer on superhydrophobic surface underwater. *Colloids and Surfaces A: Physicochemical and Engineering Aspects* 377(1), 374-378.

Song, D., B. Song, H. Hu, X. Du and Z. Ma (2015). Contact angle and impinging process of droplets on partially grooved hydrophobic surfaces. *Applied Thermal Engineering* 85, 356-364.

Song, D., R. J. Daniello and J. P. Rothstein (2014). Drag reduction using super-hydrophobic sanded teflon surfaces. *Experiments in Fluids* 55(8), 1-8.

Succi, S. (2001). *The Lattice Boltzmann Equation: For Fluid Dynamics and Beyond*. Oxford university press.

Swift, M. R., W. R. Osborn and J. M. Yeomans (1995). Lattice Boltzmann simulation of non-ideal fluids. *Physical Review Letters* 75(5).

Tian, H., J. Zhang, N. Jiang and Z. Yao (2015). Effect of hierarchical structured superhydrophobic surfaces on coherent structures in turbulent channel flow. *Experimental Thermal and Fluid Science* 69, 27-37.

Tretheway, D. C. and C. D. Meinhart (2002). Apparent fluid slip at hydrophobic microchannel walls. *Physics of Fluids* 14(3), L9-L12.

Yao, Z., P. Hao, X. Zhang and F. He (2012). Static and dynamic characterization of droplets on hydrophobic surfaces. *Chinese Science Bulletin*

57(10), 1095-1101.

Yong-Sheng, Y. and W. Qing-Ding (2006). Experimental study on physical mechanism of drag reduction of hydrophobic materials in laminar flow. *Chinese physics letters* 23(6), 1634-1637.

Yuan, P. and L. Schaefer (2006). Equations of state in a lattice Boltzmann model. *Physics of Fluids* 18(4).

Zhang, J., H. Tian, Z. Yao, P. Hao and N. Jiang (2015). Mechanisms of drag reduction of superhydrophobic surfaces in a turbulent boundary layer flow. *Experiments in Fluids* 56(9), 1-13.

Zhu, L., D. Tretheway, L. Petzold and C. Meinhart (2005). Simulation of fluid slip at 3D hydrophobic microchannel walls by the lattice boltzmann method. *Journal of Computational Physics* 202(1), 181-195.